Tellus - 1994, 46A, 149 - 159
Printed in Belgium - all rights reserved

TELLUS
ISSN 0280-6495

A model study of the Rhine discharge front and downwelling circulation

By K. G. RUDDICK†*, E. DELEERSNIJDER‡, T. DE MULDER† and P. J. LUYTEN†, †*Management Unit of Mathematical Models of the North Sea and Scheldt Estuary (MUMM), 100 Gulledelle, B-1200 Bruxelles, Belgium*; ‡*Institut d'Astronomie et de Géophysique G. Lemaitre, Université Catholique de Louvain, Chemin du Cyclotron 2, B-1348 Louvain-la-Neuve, Belgium*

(Manuscript received 2 December 1992; in final form 17 June 1993)

ABSTRACT

The Rhine is the largest river discharge of the North Sea, and has considerable ecological importance as a source of nutrients and pollutants. While much of the Dutch coastal zone is intensively monitored, it is difficult to perform measurements within the first few km of discharge, a region of very high horizontal and vertical gradients, which influences strongly the fate of freshwater and riverborne material. A fine resolution 3D hydrodynamic model, MU-ROFI, has been developed to simulate the flow in this initial discharge zone. The model is described briefly and a first set of model results is presented and discussed. The process of front formation and associated downwelling on the upstream (with respect to the tide) boundary of the freshwater plume, switching from the South to the North boundary as the tide turns, is illustrated. Qualitative comparison with CTD and airborne remotely sensed measurement indicates that such a behaviour is realistic, at least in conditions of low wind and Neap tide.

1. Introduction

The study of the hydrodynamics of freshwater plumes, is motivated by the need to understand the physical processes which govern the transport of suspended and dissolved matter discharged by rivers. The Rhine plume is of particular ecological significance, since, with an average flow of about 2200 $m^3 s^{-1}$, it is the largest river discharge of the North Sea. Heavy metals and chlorinated hydrocarbons originating from industry in the Rhine and Meuse basins reach the North Sea via the Rotterdam waterway and, in periods of high discharge, the Haringvliet Sluice, see Fig. 1a. For example, Kramer and Duinker (1988) estimate that in 1979–81, the Rhine discharge through the Rotterdam waterway supplied an average of 37 tonnes of cadmium and 4.4 tonnes of mercury per year, and Thome et al. (1992) estimate a flux of 9 tonnes per year of polychlorinated biphenyls (PCBs). In addition to toxic chemicals, the supply of biological nutrients, especially nitrates and phosphates, affects strongly the ecosystem of the southern North Sea; Gieskes and Schaub (1990) report a high correlation between Rhine discharge and phytoplankton biomass in the Dutch coastal zone.

Extensive measurement campaigns in the Dutch coastal zone have generated considerable knowledge of the hydrographic structure of the region, especially at long time scales (relative to the mesoscale) and to the North of Hoek van Holland. For example, de Ruijter et al. (1992) studied the annual average circulation and found a longshore northward residual current driven by winds, and an onshore bottom residual current arising from an estuarine cross-shore circulation. Simpson et al. (1993) observed semi-diurnal and semi-monthly periodic stratification in the Rhine ROFI (Region of Freshwater Influence) arising from variability in the tidal mixing. De Kok (1992) has used a 3D

* Corresponding author.

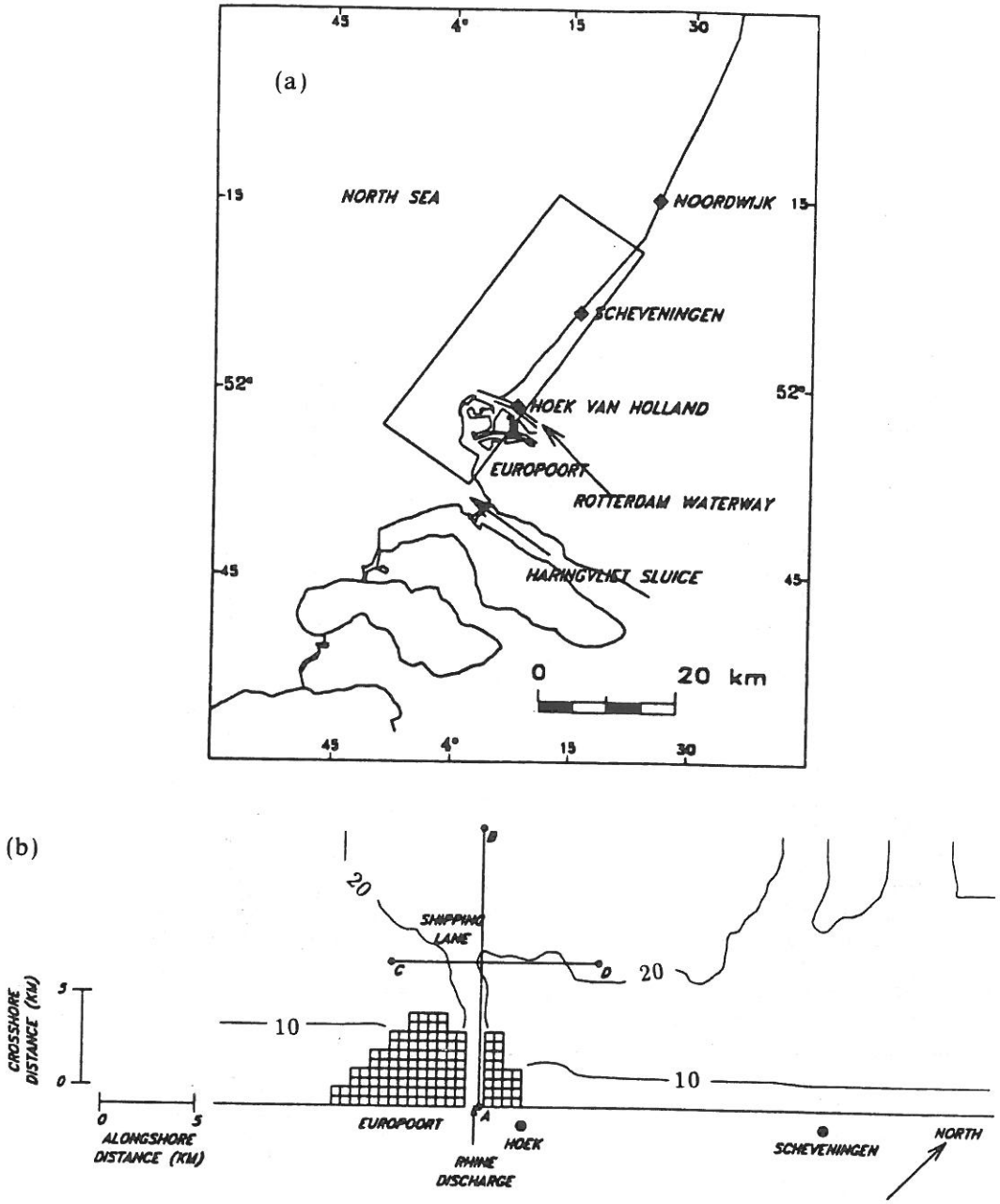

Fig. 1. (a) (Top) The region of the Rhine plume showing the domain of interest (box), the Dutch coast (lines) and the Rhine discharges at the Rotterdam waterway and the Haringvliet Sluice. (b) (Bottom) Bathymetry of the Rhine plume (courtesy of Rijkswaterstaat, Tidal Waters Division) showing isobaths (m), landmarks, and the location of the cross-shore (AB) and alongshore (CD) transects used to present results.

hydrodynamic and suspended sediment model to study the transport of dredged material within a residual gyre to the North of the waterway mouth. However, little information exists concerning the flow within a few kilometres of the waterway mouth, where van Alphen et al. (1988) suggest there is a strong mesoscale interaction between the tidal stream and the freshwater jet. Yet a thorough understanding of this region is essential for prognostic simulation of the fate of riverborne pollutants and nutrients, since the initial horizontal and vertical distribution of freshwater may strongly influence the subsequent dispersion in the Dutch coastal zone. For example, Visser, Bos and de Ruijter (personal communication) use "simple" analytic models to determine criteria on the river discharge for the formation of distinct tidal pulses of freshwater, which separate from the coast, thus enhancing considerably cross-shore exchange of nutrients and pollutants; in situ and remotely sensed measurements indicate that such patches may survive up to 30 km from the river mouth. However, little information is available on the flow near the waterway mouth, where the busy shipping lane renders in situ measurement difficult.

No attempt will be made to summarise the hydrodynamics of river plumes (e.g., Simpson and James (1986) or McClimans (1988)). Rather the aim here is to focus on a single physical process: the tidal dynamics of the discharge front and associated (secondary) downwelling circulation in the near-field, up to 10 km from the waterway mouth. The 3D hydrodynamics model MU-ROFI is described briefly in Section 2, together with the numerical discretisation and boundary conditions. The results of numerical simulations are presented in Section 3, showing the formation and disappearance of fronts on the North and South boundaries of the plume during a tidal cycle. A comparison is made with measurements made for the Rhine and similar river plumes.

2. Method

2.1. *Forcing mechanisms*

The principal forcing mechanisms affecting flow in the region of interest are:

- Tide: as is the case for much of the Southern Bight of the North Sea, mesoscale variability is dominated by the tides. At the Hoek van Holland, tidal forcing is principally M2 (amplitude of 0.77 m), modulated over the Springs-Neaps cycle by S2 (amplitude of 0.19 m). The tide propagates from the South up the Dutch coast approximately as a Kelvin wave, giving instantaneous currents of the order 1 m/s and generating turbulent vertical mixing by bottom friction.
- River: the river discharge provides a source of buoyancy, which drives density currents. Measurements by Abraham et al. (1986) and Bos (1991) show a stratified flow within the waterway with considerable tidal variability of the river discharge.
- Wind: strong winds influence plume dynamics both by interacting with the tide to influence the large-scale circulation in the Southern Bight and by locally inducing surface currents and promoting vertical mixing.

2.2. *Choice of model*

While simple "reduced-physics" models offer considerable insight into physical processes, their applicability is often severely limited by the assumptions made; since a long term aim of the work presented here is to provide the hydrodynamic forcing for water quality modelling involving biogeochemical processes, a general purpose 3D model has been developed, named MU-ROFI, retaining as much as possible of the physics present in the sea, including strong non-linearities. Thus, it becomes possible to approach more realistic simulation of a highly complex system. The price to pay for this is the difficulty of interpreting results, which will exhibit a confusion of non-linearly interacting processes over a range of time and length scales.

2.3. *Governing equations for shallow sea hydrodynamics*

The governing equations are obtained from considering conservation of mass, momentum and salinity using the Boussinesq approximation, the boundary layer approximation (including hydrostatic equilibrium) and the representation of unresolved turbulent fluctuations by an eddy viscosity and diffusivity, ν_t and λ_t. The state variables employed are the horizontal velocity, $\boldsymbol{u}$, the vertical velocity component, w, practical salinity, S, reduced pressure, q, defined as the pressure relative to a reference atmospheric pressure, $P_{atm,0}$, reduced by removal of a linear

hydrostatic pressure profile and divided by a reference density, ρ_0:

$$q = \frac{P - P_{\text{atm.0}}}{\rho_0} + g x_3. \tag{1}$$

The buoyancy, b, relative to a reference salinity, S_0, is obtained by considering a linearised equation of state, neglecting the effect of temperature variations on density, which is dominated by salinity variation for this region,

$$b = \beta_S g(S_0 - S), \tag{2}$$

where g is the gravitational acceleration and β_S the coefficient of haline expansivity. Evolution of these quantities are given for a Cartesian coordinate system (x_1, x_2, x_3) with horizontal unit vectors $\boldsymbol{e}_1, \boldsymbol{e}_2$ and vertical (upwards) unit vector $\boldsymbol{e}_3$, by (e.g., Nihoul, 1984):

$$\nabla_h \cdot \boldsymbol{u} + \frac{\partial w}{\partial x_3} = 0, \tag{3}$$

$$\frac{\partial q}{\partial x_3} = b, \tag{4}$$

$$\frac{\partial \boldsymbol{u}}{\partial t} + \nabla_h \cdot (\boldsymbol{u}\boldsymbol{u}) + \frac{\partial (w\boldsymbol{u})}{\partial x_3} - \frac{\partial}{\partial x_3}\left(\nu_t \frac{\partial \boldsymbol{u}}{\partial x_3}\right) = -f\boldsymbol{e}_3 \otimes \boldsymbol{u} - \nabla_h q, \tag{5}$$

$$\frac{\partial S}{\partial t} + \nabla_h \cdot (\boldsymbol{u}S) + \frac{\partial (wS)}{\partial x_3} - \frac{\partial}{\partial x_3}\left(\lambda_t \frac{\partial S}{\partial x_3}\right) = 0, \tag{6}$$

where the horizontal gradient operator is given by,

$$\nabla_h = \boldsymbol{e}_1 \frac{\partial}{\partial x_1} + \boldsymbol{e}_2 \frac{\partial}{\partial x_2}. \tag{7}$$

2.4. *Numerical discretization*

The governing equations (3–6) are discretised using well-established numerical methods, following closely the work of Blumberg and Mellor (1987), Beckers (1991) and Deleersnijder (1992).

Space discretisation is performed by taking conservative finite differences on a Cartesian Arakawa "C" grid, after sigma transformation of the vertical coordinate. Advection is treated by a finite difference version of the first order vector upwind scheme of Rice and Schnipke (1985). Thus, referring to the stagerred mesh illustrated in Fig. 2, the advective flux of salinity is given by (8).

$$(uS)_{i-1/2,j} = \begin{cases} u_{i,j} S_{i-1,j-1} & \text{if } v > u > 0, \\ u_{i,j} S_{i-1,j} & \text{if } u > |v| > 0 \\ u_{i,j} S_{i-1,j+1} & \text{if } -v > u > 0 \\ u_{i,j} S_{i,j-1} & \text{if } v > -u > 0 \\ u_{i,j} S_{i,j} & \text{if } -u > |v| > 0 \\ u_{i,j} S_{i,j+1} & \text{if } -v > -u > 0 \end{cases} \tag{8}$$

All terms are discretised explicitly, except for the vertical diffusion terms, which are treated implicitly. The Coriolis terms are discretised centrally over two steps using the approach of Sielecki (1968). A mode-splitting approach is used to separate calculation of the 3D structure, calculated

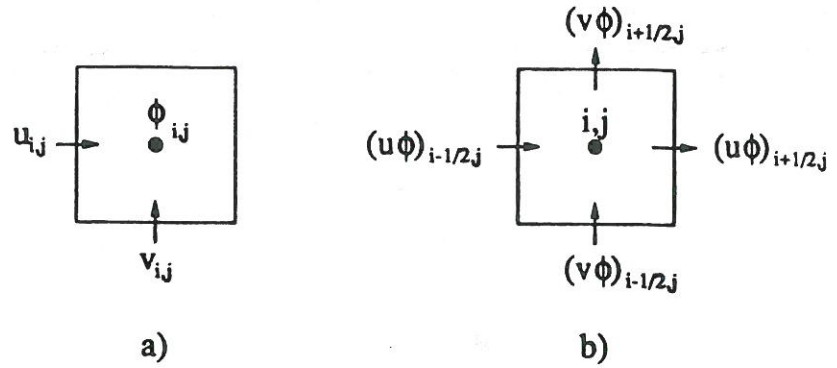

Fig. 2. Location of variables on an Arakawa-C staggered mesh: (a) Scalar ϕ and velocity components; (b) Advective fluxes of ϕ.

with time step Δt_{3D}, from the fast-moving surface gravity waves, calculated with time step Δt_{2D}, but retaining semi-implicit treatment of bottom stress in the 2D equation set.

Horizontal diffusion terms were not used for the simulations presented here, following the suggestion of Mellor and Blumberg (1985) and Deleersnijder et al. (1992) that horizontal diffusion is usually employed in marine models purely for numerical reasons (to ensure monotonicity or stability) rather than as a parameterisation of sub-grid scale processes. The numerical diffusion inherent in the advection scheme is more than sufficient for such a purpose.

2.5. *Boundary conditions*

Open sea boundary conditions are required to model the forcing from the large-scale circulation outside the domain of interest, while "allowing disturbances originating within the computational domain to leave it without disturbing or deteriorating the internal solution" (Røed and Cooper, 1986). The approach used here is based on the propagation of Riemann variables, and is inspired by the "characteristic" boundary condition of Hedstrom (1979), which performed well in the tests of Røed and Cooper (1987). At the Southern and Northern cross-shore boundaries and the offshore and river discharge boundaries, the incoming Riemann variables are imposed by conditions (9), (10), and (11) and (12) respectively.

$$U + c\eta = 2c\eta_0 \sin \omega t, \tag{9}$$

$$U - c\eta = 0, \tag{10}$$

$$V - c\eta = c\eta_0 \sin\left(\frac{\omega x}{\bar{c}} - \omega t\right), \tag{11}$$

$$V + c\eta = \frac{2}{A}\left[Q_0 - Q_1 \sin \omega t\right], \tag{12}$$

where U is the alongshore transport (in $m^2 s^{-1}$), V is the cross-shore transport, $c = \sqrt{gh}$ is the surface gravity long wave propagation speed, η the surface elevation, h the mean water depth, $\omega = 1.405 \cdot 10^{-4}$ rad s^{-1} the angular speed of the M2 tidal component, x, the distance alongshore from the Southern boundary, $\bar{c} = \sqrt{g \cdot 20\ \text{m}}$ is a typical value of c for the domain, and $\eta_0 = 0.9$ m the amplitude of the tidal forcing, $A = 1$ km a representative width for the river mouth, $Q_0 = 1200\ m^3 s^{-1}$ and $Q_1 = 1800\ m^3 s^{-1}$ the constant and tidal components of vertically-integrated discharge. The outgoing Riemann variables are computed by the compatibility relation along the characteristic leaving the domain, which is given in (13) for the offshore boundary:

$$\left(\frac{\partial}{\partial t} + c\frac{\partial}{\partial y}\right)(V + c\eta) = -c\frac{\partial U}{\partial x} + \tau^{\text{surf}} - \tau^{\text{bott}} - fU - \hat{\mathcal{A}}^{\text{h}} + \hat{\mathcal{D}}_{\text{d}}, \tag{13}$$

where τ^{surf} and τ^{bott} are the surface and bottom stress, and $\hat{\mathcal{A}}^{\text{h}}$ and $\hat{\mathcal{D}}_{\text{d}}$ are the vertical integrals of horizontal advection of momentum and internal pressure gradient respectively. Thus, computing $V + c\eta$ from (13) and imposing $V - c\eta$ from (11), the boundary transport V is obtained.

The vertical structure at open sea boundaries is allowed to develop from the internal solution, by requiring zero normal derivative of the deviation from the vertically-averaged horizontal velocity as suggested by Deleersnijder et al. (1989), and given for the offshore boundary in (14).

$$\frac{\partial}{\partial y}\left(v - \frac{V}{H}\right) = 0. \tag{14}$$

Salinity is treated at open sea boundaries by upwinding when flux is out of the domain and by supposing that incoming fluxes correspond to advecting the reference salinity S_0, except at the river discharge where a two layer vertical structure, with salinity of 5 in the upper layer and 25 in the lower layer, is applied where the flux is incoming.

The normal transport is set to zero at coastal boundaries. Bottom stress is computed using a quadratic wall-function with a roughness length, z_0 (see Table 1). Surface stress is not applied in these simulations.

2.6. *Model verification*

As a first step towards quality assurance, the model has been verified to reproduce the analytical or a documented numerical solution to a number of simple problems including the wind-forced Ekman spiral considered by Lynch and Officer (1985), the propagation of a Kelvin wave in a coastal domain (Gill, 1982), the moving storm

simulated numerically by Røed and Cooper (1987), the flow induced in a coastal domain by a uniform wind using linear bottom friction, and the advection of a "rotating cone" (Takacs, 1985). While, non-linear interactions are not tested, routine checking of these problems after every program modification helps ensure error-free code.

In an attempt to approach standardisation of models and build the basis for a water quality model of the North Sea for use as a management tool, the structured program "framework" of Wolf (1991) and the program documentation system of Gibson (1986) are used.

2.7. *Test conditions*

Simulations were performed using the bathymetry shown in Fig. 1b. The constants and parameters used are given in Table 1.

The constant eddy viscosity and diffusivity coefficients were tuned by preliminary tests, which indicate that model results are indeed sensitive to these parameters. Clearly, the use of constant coefficients is unrealistic: far from the river mouth the tidal forcing generates much stronger vertical mixing, and conversely, for strongly stratified regions in and near the estuary turbulent mixing is suppressed, and much lower diffusivities should be used. A more appropriate solution would be to model the production, dissipation and transport of turbulent kinetic energy as Mellor and Yamada (1982) and Luyten and Deleersnijder (1991).

Table 1. *Resolution, parameters and constants used in simulations*

horizontal grid	$\Delta x, \Delta y$	500 m
vertical sigma levels	$\frac{\text{depth}}{\Delta z}$	15
time step (2D)	Δt_{2D}	15 s
time step (3D)	Δt_{3D}	30 s
eddy viscosity	ν_t	$1.5 \cdot 10^{-3}$ m^2 s^{-1}
eddy diffusivity	λ_t	$1.5 \cdot 10^{-3}$ m^2 s^{-1}
roughness length	z_0	10^{-3} m
reference density	ρ_0	1027.4 kg m^{-3}
reference salinity	S_0	30
haline expansivity	β_S	$0.766 \cdot 10^{-3}$
Coriolis frequency	f	$1.146 \cdot 10^{-4}$ s^{-1}
gravitational acc.	g	9.81 m s^{-2}

Initial conditions are obtained by spinning up the model for four tidal cycles without river discharge, and then six tidal cycles with discharge, thus allowing freshwater to reach the open sea boundaries and giving time for a near-periodic solution to be reached in the near-field. The results are then presented for the following tidal cycle.

3. Results

Fig. 3 shows the flow for a cross-shore transect passing through the estuary, at the falling turn of the tide. Vectors represent a vector sum of horizontal velocity with an "upwelling" velocity, the velocity across iso-σ surfaces,

$$\tilde{w} = H\left(\frac{\partial}{\partial t} + u\frac{\partial}{\partial x} + v\frac{\partial}{\partial y} + w\frac{\partial}{\partial z}\right)\left[\frac{z+h}{\eta+h}\right], \qquad (15)$$

where $H = \eta + h$ is the total water depth, and h the mean water depth. This upwelling velocity $\tilde{w}$ is recommended by Deleersnijder (1989) as giving a clearer representation of true upwelling processes than the physical vertical velocity, since the "upsloping" component of flow arising from stretching or squashing by the bottom and surface topography has been removed. The first four kilometres of this transect lie within the waterway, where a two layer salt wedge flow can be clearly distinguished. At the mouth of the waterway very high gradients of salinity and horizontal and upwelling velocity components occur as seen in Fig. 3; realistic modelling of the flow at the mouth itself is particularly difficult because of the small length scales involved (significantly smaller than the grid size of 500 m used here) and the influence of the complex harbour geometry.

An idea of the respective importance of the processes influencing subsequent spreading in the near-field (10 km) of the river mouth can be found by evaluating a posteriori the (vertical) Peclet number, Pe, the densimetric Froude number, Fr, and the internal Rossby radius, Ro. Taking characteristic scales for upwelling velocity, $W \sim 5 \cdot 10^{-4}$ m s^{-1}, vertical length scale of the stratified region, $L_z \sim 5$ m, vertical eddy diffusivity,

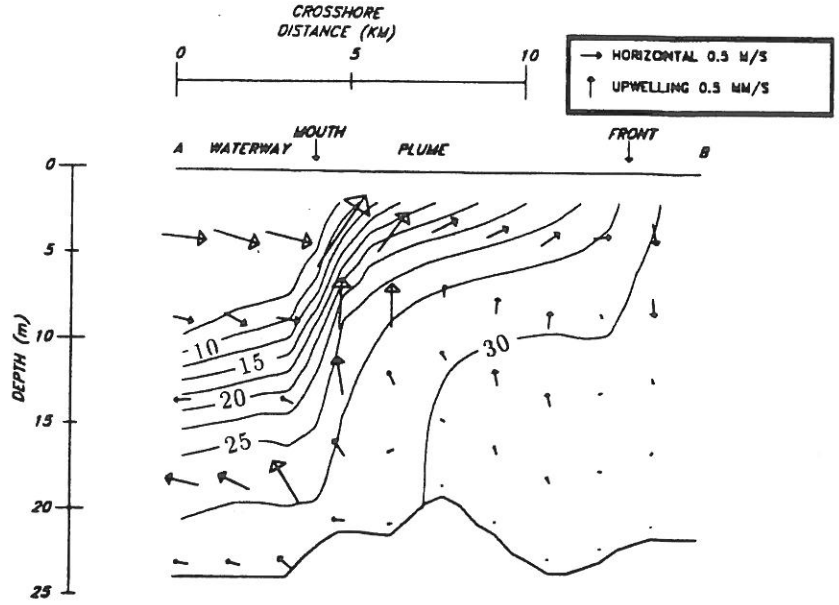

Fig. 3. Cross-shore transect AB showing the two-layer salt wedge flow within the waterway, and subsequent buoyant spreading combined with vertical mixing. Contours show isohalines (practical salinity units) and vectors are plotted for one in every three points.

$\lambda_t \sim 1.5 \cdot 10^{-3}\ \mathrm{m^2\,s^{-1}}$, horizontal velocity, $U \sim 0.5\ \mathrm{m\,s^{-1}}$, and buoyancy, $B \sim 0.06\ \mathrm{m^1\,s^{-2}}$ gives:

$$\mathrm{Pe} = \frac{\text{vertical advection}}{\text{vertical diffusion}} = \frac{WL_z}{\lambda_t} \sim 1.7, \qquad (16)$$

$$\mathrm{Fr}^2 = \frac{\text{kinetic energy}}{\text{potential energy}} = \frac{U^2}{BL_z} \sim 0.8, \qquad (17)$$

$$\mathrm{Ro} = \frac{\text{internal long-wave speed}}{\text{Coriolis frequency}} = \frac{\sqrt{BL_z}}{f} \sim 5\ \mathrm{km}. \qquad (18)$$

Thus, since both Fr and Pe are of order one both near-critical buoyant spreading and vertical

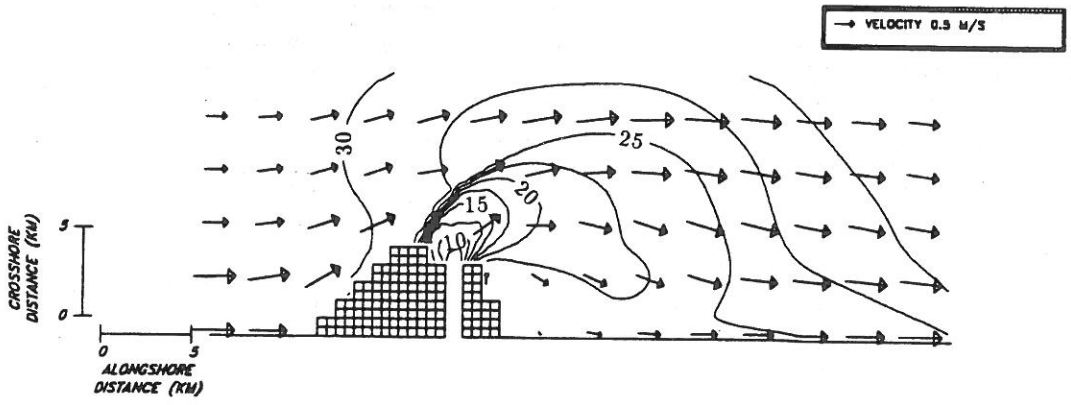

Fig. 4. Surface currents and salinity (practical salinity units) at high tide (plotting 1 in every 6 vectors in both directions).

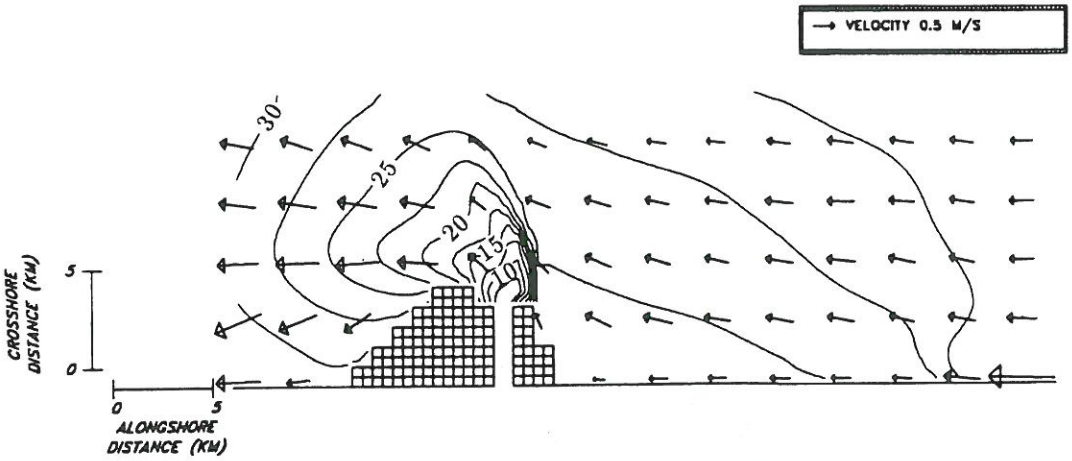

Fig. 5. Surface currents and salinity (practical salinity units) at low tide (plotting 1 in every 6 vectors in both directions).

mixing influence the subsequent thinning of the upper layer. At distances further from the mouth, as the horizontal length scale, L_h, approaches Ro, rotational effects become important as the flow adjusts to quasi-geostrophy.

The flow in this cross-shore plane is qualitatively similar throughout the tidal cycle. The tidal variation in surface velocity ($1.2\ m\ s^{-1} \pm 0.2\ m\ s^{-1}$) in the estuary is much smaller than typical measured values, where current reversal is observed for about 3 h around high tide, implying that the river boundary condition currently employed needs considerable improvement.

Fig. 4 shows surface currents and salinity at high tide. Freshwater emerging from the waterway interacts with the tidal stream, which impedes gravitational spreading on the upstream (South) plume boundary and, together with the Coriolis deflection enhances spreading in the downstream direction. While, realistically, a particularly strong front is formed in the first few kilometres of discharge, where surface practical salinity gradients of $10^{-2}\ m^{-1}$ occur , subsequent weakening of this front further from the river mouth may be significantly affected by the numerical diffusion introduced by the advection scheme (a typical horizontal velocity of $0.2\ m\ s^{-1}$ implies a numerical diffusion coefficient of order $50\ m^2\ s^{-1}$). A second, and more daunting, obstacle to sharp resolution of fronts is the lack of horizontal resolution (both in models and measurements) since visual observations of the water colour in this region indicate discontinuites with a cross-front length scale of only a few metres, representation of such a poorly understood, small scale, and possibly non-hydrostatic, feature is clearly beyond the scope of the present study.

There is some similarity between results presented here and the numerical simulations of Chao and Boicourt (1986) of a rotating plume discharging into non-tidal waters; however the formation of the coastal buoyancy current present in their simulations is underrepresented here, because of the proximity of tidally forced open sea boundaries. Formation of a sharp discharge front, curving downstream, has been shown by Garvine (1987) for a non-rotating plume from a river outlet normal to the coast; again the domain would need to be significantly extended to study the meandering coastal front predicted by Garvine.

At low tide (Fig. 5), a front builds up on the Northern plume boundary, with lateral spreading to the South. Here the front is oriented more perpendicularly to the coast than at high tide, since Coriolis deflection now opposes the tidal stream. The two lobe structure seen in the surface salinity field, 2 km from the mouth, is caused by the deep shipping channel. This pattern of front formation on the upstream boundary of a tidally-forced river plume is remarkably similar to the surface salinity observations of the Connecticut river plume made by Garvine (1974), which show switching of the front from the left to the right plume boundary going from high to low tide.

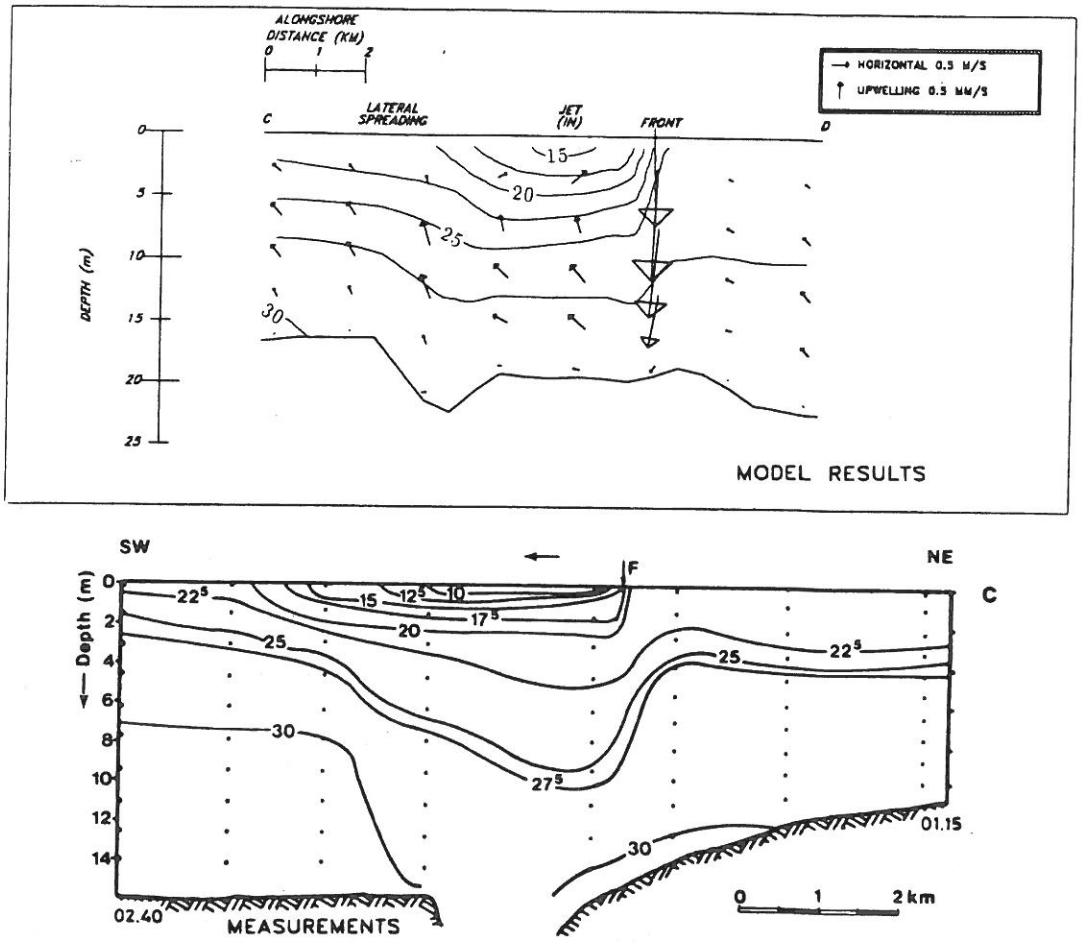

Fig. 6. Velocity and salinity (practical salinity units) through the along-shore transect CD at the rising turn of the tide, compared to CTD measurements (reproduced from Van Alphen et al. (1988) ©Springer-Verlag). Vectors are plotted for one in every three points.

The flow in the plane parallel to the coast at the rising turn of the tide is illustrated in Fig. 6 in comparison with CTD measurements by van Alphen et al. (1988). Surfacing isohalines concentrate at a front; the associated convergence and downwelling circulation (with downwelling velocities in excess of $2 \cdot 10^{-3}$ m s^{-1}) is reponsible for the accumulation of surface matter reported marking this front. Such a structure has been suggested by Imberger (McClimans, 1988, Fig. 4) and observed by Garvine (1977) for the Connecticut river plume. This characteristic circulation in the plane perpendicular to the freshwater jet is schematised in Fig. 7 for the non-rotating regime ($L_h < \mathrm{Ro}$) of the plume.

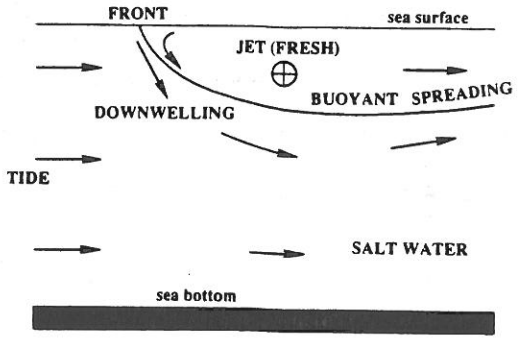

Fig. 7. Schematic along-shore transect of near-field spreading of the river plume as a freshwater jet impinging normally on the tidal stream.

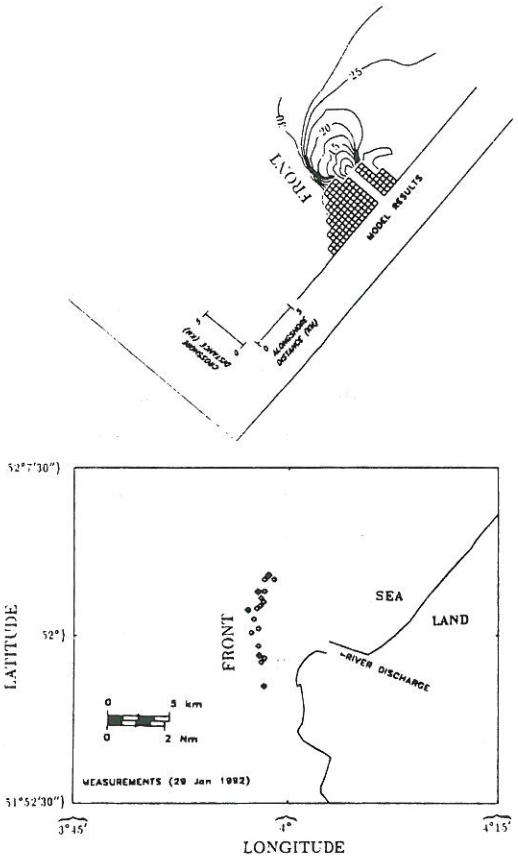

Fig. 8. Comparison between model results for surface salinity (practical salinity units) and the front location determined by airborne remote sensing (visual/video observations as open squares; radar measurements as full squares), falling (Neap) tide.

A further comparison with SLAR (Side-Looking Airborne Radar) and visual measurement of the front location on the falling (Neap) tide in calm conditions, made with the help of the BELMEC (Belgian Marine Environmental Control) team, is shown in Fig. 8.

4. Conclusions

A 3D numerical model is used to study the process of front formation in the near-field of the discharge of the river Rhine into the North Sea. The model is described briefly. Preliminary results give a clear illustration of the process of front formation and strong downwelling at the upstream (with respect to the tide) boundary of the plume; as the tide turns from high to low the Southern plume boundary front weakens and a front forms on the Northern plume boundary. A qualitative comparison with measurements made by CTD and airborne remote sensing indicates that such a behaviour is realistic, at least in conditions of low wind and Neap tide. Future model developments include a turbulence closure model, a less diffusive advection scheme, and an improved treatment of the river discharge boundary condition, thus enabling more realistic treatment of vertical diffusion processes, resolution of sharper fronts, and investigation of the pulsed nature of the Rhine outflow.

5. Acknowledgements

K. G. Ruddick and P. Luyten were funded by the European Community under contracts MAST-900064 and MAST-0050-C ("PROFILE") respectively. Colleagues in the PROFILE group are thanked for many helpful discussions during workshops and informal meetings; in particular, J. de Kok is acknowledged for advice on modelling the Rhine plume. The CAMME (Computer Assisted Management of the Marine Environment) team is thanked for providing computing resources and prompt user support. Finally, J. Ozer is thanked for constructive criticism throughout the course of this study, and L. P. Røed for advice on open sea boundary conditions.

REFERENCES

Abraham, G., de Jong, P. and Van Kruiningen, F. E. 1986. Large-scale mixing processes in a partly mixed estuary. *Technical Report 371*, Delft Hydraulics.

Beckers, J. M. 1991. Application of the GHER 3D general circulation model to the Western Mediterranean. *J. Mar. Sys.* **1**, 315–332.

Blumberg, A. F. and Mellor, G. L. 1987. A description of a three-dimensional coastal ocean circulation model. In: *Three-dimensional coastal ocean models* (ed. Heaps, N. S.). Washington DC, American Geophysical Union, 1–16.

Bos, W. G. 1991. A comparison of two doppler current profilers. *IEEE J. Oceanic Engin.* **16**, 374–381.

Chao, S. Y. and Boicourt, W. C. 1986. Onset of estuarine plumes. *J. Phys. Oceanogr.* **16**, 2137–2149.

De Kok, J. M. 1992. A 3D finite difference model for the

computation of near- and far-field transport of suspended matter near a river mouth. *Cont. Shelf Res.* **12**, 625–642.

De Ruijter, W. P. M., Van der Giessen, A. and Groenendijk, F. C. 1992. Current and density structure in the Netherlands coastal zone. In: *Dynamics and exchanges in estuaries and the coastal zone* (ed. Prandle, D.), vol. 40, *Coastal and estuarine studies*. New York, Springer-Verlag, 529–550.

Deleersnijder, E. 1989. Upwelling and upsloping in three-dimensional marine models. *Appl. Math. Modelling* **13**, 462–467.

Deleersnijder, E. 1992. Modélisation hydrodynamique tridimensionnelle de la circulation générale de la région du détroit de Bering. PhD thesis, Université Catholique de Louvain, Louvain-La-Neuve, Belgium.

Deleersnijder, E., Norro, A. and Wolanski, E. 1992. A three-dimensional model of the water circulation around an island in shallow water. *Cont. Shelf Res.* **12**, 891–906.

Deleersnijder, E., Wolanski, E. and Norro, A. 1989. Numerical simulation of the three-dimensional tidal circulation in an island's wake. In: *Computers and experiments in fluid flow* (eds. Carlomango, G. M. and Brebbia, C. A.). Springer-Verlag, 355–381.

Garvine, R. W. 1974. Physical features of the Connecticut river outflow during high discharge. *J. Geophys. Res.* **79**, 831–846.

Garvine, R. W. 1977. Observations of the motion field of the Connecticut river plume. *J. Geophys. Res.* **83**, 441–454.

Garvine, R. W. 1987. Estuary plumes and fronts in shelf waters: a layer model. *J. Phys. Oceanogr.* **17**, 1877–1896.

Gibson, J. K. 1986. *Standards for software development and maintenance*. Technical Report 120, European Centre for Medium Range Weather Forecasting, Shinfield Park, Reading, UK.

Gieskes, W. W. C. and Schaub, B. E. M. 1990. Correlation of the seasonal and annual variation of phytoplankton biomass in Dutch coastal waters of the North Sea with Rhine river discharge, vol. 36, *Coastal and estuarine studies*. New York, Springer-Verlag, 311–320.

Gill, A. E. 1982. *Atmosphere-ocean dynamics*. Academic Press, 378–380.

Hedstrom, G. W. 1979. Nonreflecting boundary conditions for nonlinear hyperbolic systems. *J. Comp. Phys.* **30**, 222–237.

Kramer, K. J. M. and Duinker, J. C. 1988. The Rhine/Meuse estuary. In: *Pollution of the North Sea, an assessment* (eds. Salomons, W., Bayne, B. L., Duursma, E. K. and Förstner, U.). Springer-Verlag, 194–212.

Luyten, P. J. and Deleersnijder, E. 1991. *Presentation of three turbulence models for stratified flows using $k-\varepsilon$ theory*. MAST-0050-C Technical Report 6, MUMM, Brussels, Belgium.

Lynch, D. R. and Officer, C. B. 1985. Analytic test cases for 3D hydrodynamic models. *Int. J. Num. Methods Fluids* **5**, 529–543.

McClimans, T. A. 1988. Estuarine fronts and river plumes. In: *Physical processes in estuaries* (eds. Dronkers, J. and Van Leussen, W.). Springer-Verlag, 55–69.

Mellor, G. L. and Blumberg, A. F. 1985. Modelling vertical and horizontal diffusivities with the sigma coordinate system. *Mon. Wea. Rev.* **113**, 1379–1383.

Mellor, G. L. and Yamada, T. 1982. Development of a turbulent closure model for geophysical fluid problems. *Rev. Geophys. Space Phys.* **20**, 851–875.

Nihoul, J. C. J. 1984. A three-dimensional general marine circulation model in a remote sensing perspective. *Annales Geophysicae* **2**, 433–442.

Rice, J. G. and Schnipke, R. J. 1985. A monotone streamline upwind finite element method for convection dominated flows. *Comp. Meth. Appl. Mech. Engin.* **48**, 313–327.

Røed, L. P. and Cooper, C. K. 1986. Open boundary conditions in numerical ocean models. In: *Advanced physical oceanographic numerical modelling* (ed. O'Brien, J. J.). Reidel, 411–436.

Røed, L. P. and Cooper, C. K. 1987. A study of various open boundary conditions for wind-forced barotropic numerical ocean models. In: *Three-dimensional models of marine and estuarine dynamics* (eds. Nihoul, J. C. J. and Jamart, B.). Elsevier, 305–336.

Sielecki, A. 1968. An energy-conserving difference scheme for the storm surge equations. *Mon. Wea. Rev.* **96**, 150–156.

Simpson, J. H., Bos, W. G., Schirmer, F., Souza, A. J., Rippeth, T. P., Jones, S. E. and Hydes, D. 1993. Periodic stratification in the Rhine ROFI in the North Sea. *Oceanologica Acta* **16**, 23–32.

Simpson, J. H. and James, I. D. 1986. Coastal and estuarine fronts. In: *Baroclinic processes on continental shelves* (ed. Mooers, C. N. K.). Washington DC, American Geophysical Union, 63–93.

Takacs, L. L. 1985. A two-step scheme for the advection equation with minimised dissipation and dispersion errors. *Mon. Wea. Rev.* **113**, 1050–1065.

Thome, J.-P., Hugla, J.-L. and Joiris, C. 1992. Transfert des PCBs vers la Mer du Nord: distribution dans les differents compartiments de l'ecosystème. *Bull. Soc. Roy. Sci. Liège* **61**, 99–111.

Van Alphen, J. S. L. J., De Ruijter, W. P. M. and Borst, J. C. 1988. Outflow and three-dimensional spreading of Rhine river water in the Netherlands coastal zone. In: *Physical processes in estuaries* (eds. Dronkers, J. and Van Leussen, W.). Springer-Verlag, 70–92.

Wolf, J. 1991. *A unified framework for water quality modelling in shallow seas*. Technical Report 19, Proudman Oceanographic Laboratory, Bidston, UK.